

Prediction of Weather Induced Background Radiation Fluctuation with Recurrent Neural Networks

Zheng Liu^{a,*}, Clair J. Sullivan^a

^a*University of Illinois at Urbana-Champaign*

Abstract

Background radiation estimation plays an important role in the anomalous radiation detection. Accurately estimating temporal and spatial fluctuations of background radiation helps to reduce the false alarm rate and improve the estimation accuracy of anomalous source location. It has been long observed that background radiation is positively correlated with precipitation due to the scavenging effect of rain and snow. This paper presents the usage of recurrent neural networks to predict the background radiation level based on past weather and radiation data. Two datasets are prepared with different noise levels. Experiment results show that recurrent neural networks outperform the traditional moving average algorithm on the high noise dataset; recurrent neural networks perform as well as the moving average algorithm on the low noise dataset.

Keywords: environment radiation estimation, recurrent neural network

1. Introduction

Anomalous radioactive source detection plays a major role in national security. This task includes identifying illicit movement of special nuclear materials (SNM), locating unusual radioactive events, and estimating the intensity of radioactive sources to name a few. Different algorithms, such as maximum likelihood estimation based algorithms [1, 2, 3, 4] and Bayesian estimation based algorithms [5, 6], have been developed to estimate the location and intensity of anomalous radioactive sources. Besides the anomalous radioactive sources, there exist naturally occurring radioactive materials (NORM) in the environment, and those NORM form the background radiation. The background radiation is assumed to be known in above anomalous source detection algorithms. To accurately detect and locate anomalous sources, a good understanding and estimation of background radiation is required by those algorithms.

The background radiation fluctuates with time. Studies have long observed that precipitation is positively correlated with the elevation of background radiation [7, 8]. During rainfall, background radiation increases mostly due to the scavenging effect of rain and snow that

brings radioactive materials in the upper air down to the ground [9]. ^{214}Pb and ^{214}Bi are major contributors to the elevated background radiation, and the radiation fluctuation peaks usually have a duration of several hours according to those isotope's half life[9, 8]. Stationary radiation detectors are used to monitor the background radiation, and a moving average algorithm is widely used to estimate the current background radiation from previous radiation measurements [10]. However, no weather data are utilized in the moving average method. This paper explores the usage of weather measurements together with radiation measurements to improve the estimation accuracy of the background radiation.

In this paper, recurrent neural networks (RNN) are used to predict background radiation levels based on previous background radiation measurements and weather data. Prediction results are compared between the RNN methods and the moving average method.

2. Data collection methodology

Raw data were collected by a stationary radiation detector and a weather station. The stationary detector was a $2\text{X}4\text{X}16 \text{ in}^3$ NaI(Tl) detector. It recorded background radiation spectra once every three seconds, and each of the measurement lasted for one second. Under different weather conditions, background radiation

*Corresponding author

Email address: zliu86@illinois.edu (Zheng Liu)

measurements have diverse shapes in spectra, as well as different total radiation count rates (known as gross count rate). This study focuses on the gross count rate of background radiation. For each measurement, the spectrum was summed and then divided by the measurement time to obtain the gross count rate. The unit of gross count rate is count per second (cps). This stationary detector was placed on the roof of a one-story building. A weather station was setup near the stationary detector. It collected temperature, humidity, atmospheric pressure, precipitation, wind speed and wind direction in every ten minutes.

Figure 1 shows a nine-day example of background radiation and weather measurements. The plot in the first row of Figure 1 shows background radiation measurements versus time. The dots in this plot indicate the raw measurements, while the line denotes the radiation mean value within a centered-10min time window. Because radiation gross counts intrinsically follow the Poisson distribution, those counts always fluctuate around their mean value. The plots in the following rows in Figure 1 show various weather features versus time. Several rain events occurred during this period. In each of the rain events, the background radiation can be seen to be significantly elevated.

The raw dataset consists of measurements from Dec. 21, 2016 to April 06, 2017. The whole dataset’s correlation matrix is shown in Figure 2. Temperature, humidity, air pressure, and precipitation were more correlated with background radiation than wind direction and wind speed. One possible explanation is that the fluctuation of background radiation is closely related to rains. During rains, temperature, humidity, atmospheric pressure, and precipitation level change significantly, whereas wind direction and speed are indirectly associated with the occurrence of rains. Based on the low correlation with background radiation, wind speed and wind direction were eliminated from the model.

3. Methods

3.1. Recurrent Neural Networks

Recurrent neural networks (RNNs) are designed to capture temporal contextual information along time-series data. Different from traditional feed-forward neural networks (FFNNs), RNNs have cycles in their structure that feed output from previous time steps into the current time step as input. This structure enables RNNs to model complex temporal contextual information along time series data. The back-propagation through time (BPTT) technique is usually used to train

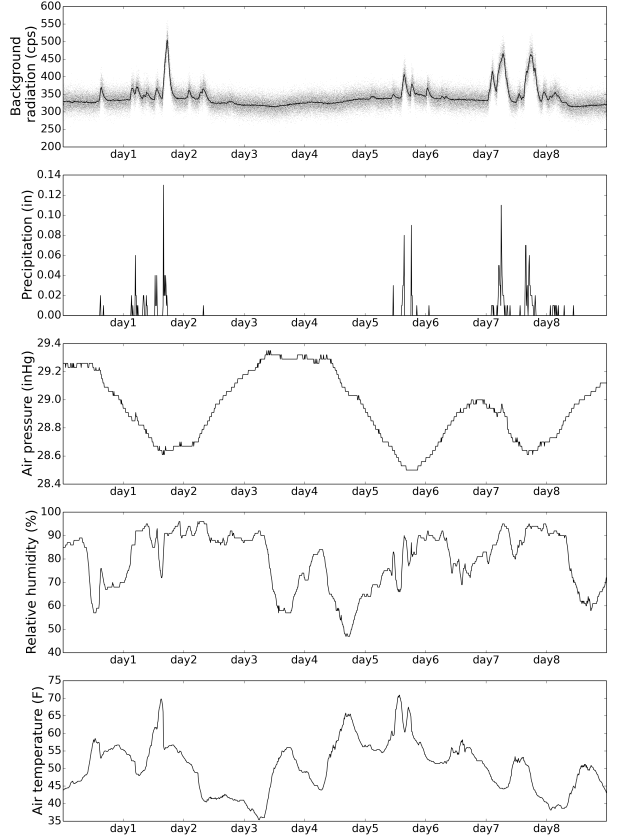


Figure 1: Background radiation and weather measurements for nine days. The top plot shows the radiation measurements (dots) and the mean radiation value (line). The subsequent plots show different weather features as they vary with time.

RNNs [11]. However, it is difficult to use BPTT to train traditional RNNs because of the gradient vanishing and exploding problem [12]. Errors from later time steps are difficult to propagate back to previous time steps and make proper updates of network parameters. To address this problem, the long short-term memory (LSTM) unit has been developed [13, 14]. The LSTM has a basic structure called a memory cell to remember and propagate unit outputs between different time steps explicitly. The LSTM memory cell uses cell states to remember temporal contextual information. It also has an input gate, an output gate, and a forget gate to control information flow between different time steps. In this study, LSTM neural networks were used to predict background radiation from time-series weather and radiation data.

Raw data of background radiation and weather measurements were first pre-processed before being fed into RNNs. In order to speed up training process and save

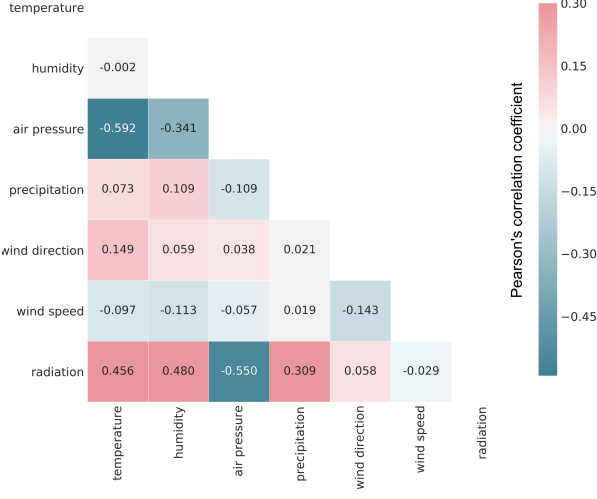


Figure 2: Correlation matrix of the background radiation and weather features.

computation resources in training RNNs, the time frequency of radiation and weather measurements were down-sampled from every 3 seconds to every minute. It is valid to downsample the time frequency because weather conditions and Poisson means of background radiation can be assumed to be approximately constant within one minute. This also makes our algorithm suitable for low-resolution measurements. Two different datasets, the dataset A and the dataset B, were obtained using different down-sampling procedures. The dataset A generated each minute’s measurement by keeping the first measurement in that minute and dropping the other measurements. The dataset B generated each minute’s measurement by taking the average of all the measurements within that minute. The dataset A is a down-sampled version of the raw dataset with sampling rate 0.05, while the dataset B is an averaged version of the raw dataset. The dataset A is noisier than the dataset B. Different RNNs were trained on the dataset A and dataset B separately, and their performances were compared in the results section.

In the preliminary test, RNNs with one hidden LSTM layer were incapable of learning the radiation and weather model due to their relatively simple structures, while RNNs with three hidden LSTM layers were too complex that they tended to overfit the data severely. As shown in Figure 3, RNNs used in this paper had an input layer, two hidden LSTM layers, and a fully connected output layer. For the training example at time step t , the input data contained background radiation and weather measurements between $t - T_{BPTT}$ and t ,

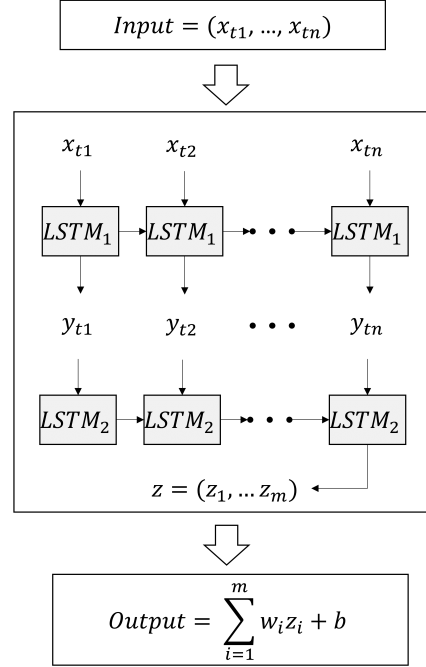


Figure 3: The RNN structure used in this paper. The input are time series data with n time steps: (x_{t1}, \dots, x_{tn}) . The first LSTM layer, $LSTM_1$, processes those n time steps data (x_{t1}, \dots, x_{tn}) and outputs an intermediate result (y_{t1}, \dots, y_m) . The second LSTM layer, $LSTM_2$, processes (y_{t1}, \dots, y_m) and outputs a vector with dimension of m : $z = (z_1, \dots, z_m)$. The output layer is a fully connected layer that calculates the weighted average of z and adds a bias b .

and the output data were the predicted radiation mean value for time step t . T_{BPTT} was the predefined time window parameter used in the BPTT algorithm. The LSTM layers were constructed using the default LSTM unit in the Keras package, which is based on the LSTM structure presented in paper [15]. The activation function was $tanh$, and the recurrent activation function was $hard - sigmoid$. Dropouts were used in two LSTM layers to avoid overfitting and to generalize the RNN model [16]. To facilitate hyper parameter tuning, a random search strategy was used to determine output dimensions and dropout rates in two LSTM layers [17]. In the random search strategy, several trials were conducted with randomly selected hyper parameters. In each trial, a neural network with randomly selected hyper parameters was trained and validated. Among those random trials, the model with the highest validation score was selected as the best model. Compared with traditional methods such as manually tuning by grid search, the random search is more efficient in hyper parameter tun-

ing [17]. The output dimension of each LSTM layer was uniformly sampled in [16, 64, 256, 1024], the dropout rates were uniformly sampled in [0, 0.5], and a total of 50 trials were applied for each experiment configuration. After two hidden LSTM layers, all the activations from the second LSTM layer were fed into the output layer. The output layer contained a single node, and no activation function was used. The output layer calculated the weighted summation of previous layer's activations as the output of the neural network. The loss function L used in the training process was the mean squared error (MSE)

$$L = \frac{1}{n} \sum_{t=1}^n (y_t - \hat{y}_t)^2 \quad (1)$$

where y_t is the radiation mean value, and \hat{y}_t is the predicted radiation mean value. Additionally, the mean absolute error

$$Error_{mean} = \frac{1}{n} \sum_{t=1}^n |y_t - \hat{y}_t| \quad (2)$$

and the maximum absolute error

$$Error_{max} = \max_t |y_t - \hat{y}_t| \quad (3)$$

were used for evaluation where y_t is the radiation mean value, and \hat{y}_t is the predicted radiation mean value from either RNN or moving window method.

In the training process, the BPTT algorithm was used to propagate the error of each layer and to update weight matrix and activation parameters [11]. The Adam optimizer was used in the gradient optimization process with recommended parameters in Kingma and Ba's paper [18]. The RNNs were trained in the stateless manner such that memory cell states were reset between different training examples. Computations were done using a single Nvidia Tesla K80 GPU with the TensorFlow package [19] as the back end and the Keras package [20] as the front end. For the total 105 days of data, seven days of data were used as testing data, and the remainder were used as training/validation data.

3.2. RNNs with Radiation Data

Besides the RNNs that used both weather and radiation measurements as input data, we also trained and tested RNNs that used only radiation measurements as input data. All other settings of these RNNs were the same as those described in the previous section.

3.3. Moving Average Method

This study also compared the performance of RNNs with the widely-used moving average method in radiation detection field [10]. In the moving average method, the time step t 's radiation mean value is predicted by taking the average of previous background radiation measurements between t and $t - T_{BPTT}$. T_{BPTT} is the same time window used in the RNN model. No weather information is used in this method.

4. Results and Discussion

This paper evaluated and compared three methods' performances on the task of estimating the mean value of current background radiation from previous radiation and weather measurements. These three methods are: RNNs with input of radiation and weather data, RNNs with input of radiation data, and the moving average method. By comparing the moving average model with the RNNs with input of radiation data, we evaluated the effectiveness of the RNN structure in reference to the moving average model. By comparing different RNN models that take different input data (radiation v.s. radiation plus weather), we evaluated the contribution of weather measurements in predicting future radiation values. Two specific questions were addressed in this section: (1) how those methods performed on different data qualities; (2) how those methods performed on different time windows. The first question is of interest because in real applications data from various measurement platforms are in different qualities. The second question is of interest because the length of time windows is hard to choose. A method will be preferred if its time window length can be set easily on a wide range of application scenarios.

Section 4.1 explains the details of different experiment configurations. Section 4.2 presents an example of background radiation prediction from the RNN model with input of radiation and weather data, the RNN model with input of radiation data, and the moving average model. Section 4.3 summarizes those models' performances on different data qualities and different lengths of time windows.

4.1. Systems and Evaluations

Several different experiment configurations were used to test the RNNs' performance on different data qualities and different time windows. As discussed in Section 3.1, the RNNs were trained and evaluated on two different datasets: the dataset A and the dataset B. The dataset A represented measurements with a high

noise level, whereas the dataset B represented measurements with a low noise level. For each dataset, 6 different time windows were tested separately: $T_{BPTT} \in [1\text{min}, 3\text{min}, 6\text{min}, 10\text{min}, 20\text{min}, 40\text{min}]$. In total, 12 different experiment setups were tested (2 different datasets x 6 different time windows) for three different models. The performances of the RNNs and the moving average method were evaluated by two metrics: the mean absolute error shown in Equation 2 and the maximum absolute error shown in Equation 3. The mean absolute error represented the mean prediction performance on the testing dataset, while the maximum absolute error represented the worst prediction case among the testing dataset. The optimized RNN structures for different experiment configurations were selected through a random search procedure. Detailed RNN configurations are listed in Appendix A.

4.2. An Example of Background Radiation Prediction

This section presents the result of background radiation prediction on the time window of 6min. With this predefined time window, the RNN model with input of radiation and weather data, the RNN model with input of radiation data, and the moving average model were trained and tested with the dataset A and the dataset B.

Figure 4 shows the background radiation estimation results of the RNN models and the moving average method on different data qualities. All the methods achieved a lower estimation error with the low noise dataset than those with the high noise dataset. For both datasets and all the methods, the maximum prediction error occurred between time index 500 and 750, during which a raining event happened. Table 1 summarizes the performance of the two RNN methods and the moving average method on the time window of 6 minutes. When the input dataset was noisy (such as Dataset A), the RNN with radiation and weather data achieved the lowest mean and maximum prediction error. With noisy dataset, RNN structures showed advantages of generating more accurate radiation predictions than the moving average method, especially for predictions in raining events. Besides, adding weather data into RNN models further reduced mean and max prediction errors. However, those advantages of RNNs didn't hold for low noise dataset (such as Dataset B). When the input dataset had radiation measurements with low noise, the moving average method achieved the lowest mean prediction error, and the RNN method with radiation data achieved the lowest maximum prediction error. This implies that for a clean enough dataset (such as Dataset B), a simple moving average operation over radiation

measurements is good enough for predicting future radiations when the time window is 6 minutes. With radiation data as input, the RNN model was able to compete with the moving average method. With radiation and weather data as input, the performance of the RNN model on low noise dataset significantly dropped. This implies that weather data brought more noise than information into the clean radiation dataset. Under this situation, the RNN model overfitted to the training data and performed poorly on the testing dataset. One possible solution to the overfitting issue is to collect more data in raining events such that RNNs can learn the relationship between raining and radiation better.

4.3. Background Radiation Prediction on Different Time Windows

Figure 5 plots the mean prediction error of the RNNs and the moving average method under different experiment configurations. As expected, both RNNs and the moving average method obtained a lower mean prediction error with the low noise dataset than those using the high noise dataset. When the time window increased, the mean prediction errors from both the RNNs and the moving average method first decreased and then converged to a low value. This is because longer time window contains more measurements. Prediction errors from Poisson statistical fluctuations are suppressed by the increased number of measurements. On the high noise dataset, the RNNs outperformed the moving average method at all time windows, and the RNNs with radiation and weather data outperformed the RNNs with radiation data at all time windows. On the low noise dataset, the difference in mean prediction errors between these three methods are less than 0.6 cps for all time windows. Under the metric of mean prediction error, the RNNs and the moving average method performed equally well on the low noise dataset.

Figure 6 shows the maximum prediction error of the RNNs and the moving average method under different configurations. As with the mean prediction error, both the RNN method and the moving average method obtained a lower maximum prediction error on the low noise dataset than the high noise dataset. As the time window increased, the maximum prediction error from the RNNs first decreased and then converged to a low level. However, the moving averaged method's maximum prediction error first decreased and then increased as the time window increased. This is because the maximum prediction error occurred in precipitations. As shown in Figure 1, background radiation would first increase and then decrease during the period of precipitation. The moving average method would under estimate

Table 1: Prediction performance for the RNN with radiation and weather data ($\text{RNN}(r, w)$), the RNN with radiation data ($\text{RNN}(r)$), and the moving average method (MA) when the time window is 6 minutes. Error unit is count per second (cps).

Prediction Error	High noise			Low noise		
	$\text{RNN}(r, w)$	$\text{RNN}(r)$	MA	$\text{RNN}(r, w)$	$\text{RNN}(r)$	MA
Mean error	3.85	4.98	5.49	1.55	1.42	1.28
Maximum error	20.71	22.08	43.41	17.06	8.41	8.47

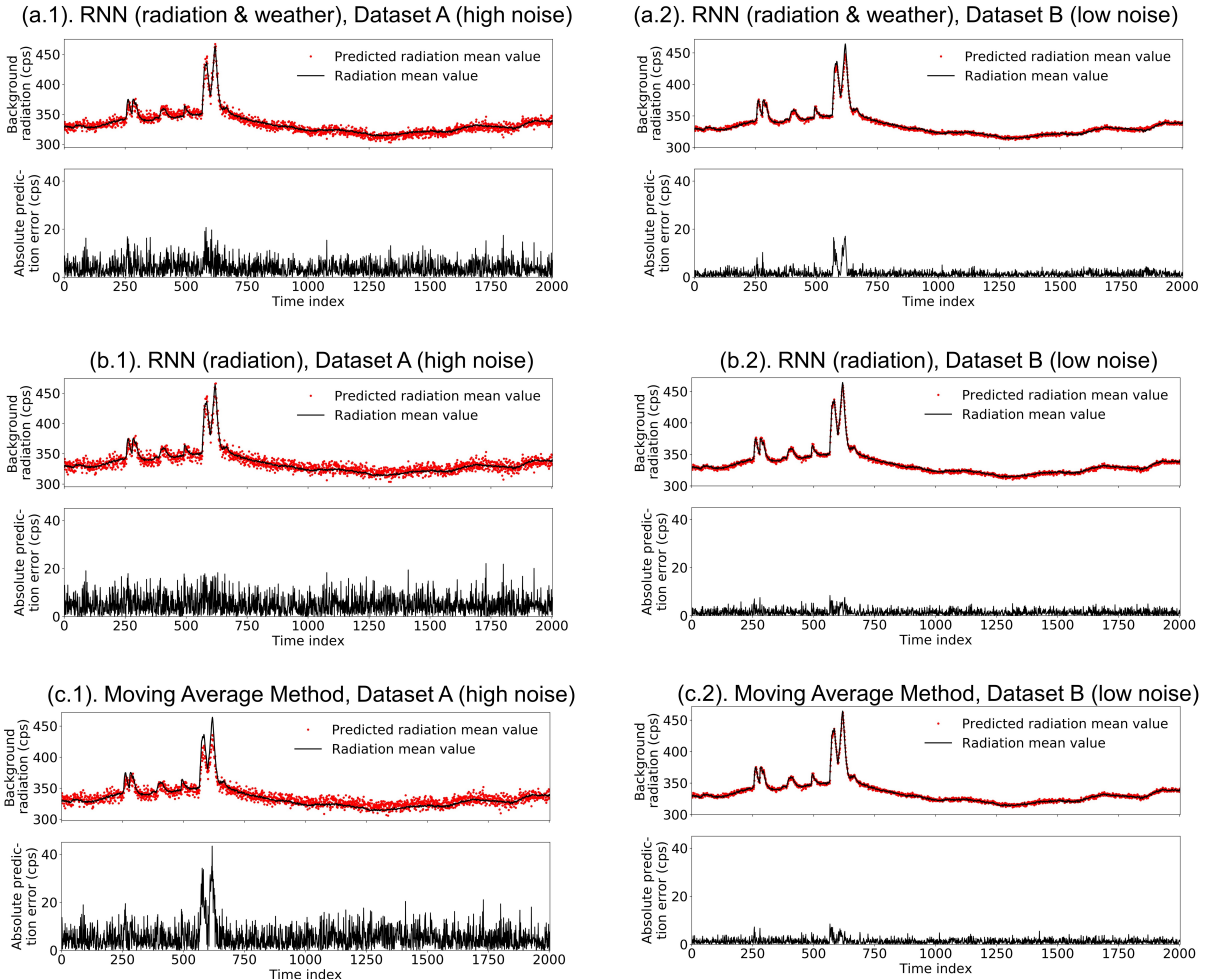


Figure 4: Performance of Background radiation estimation from the RNN methods and the moving average method. Plots in the first column use the high noise dataset. Plots in the second column use the low noise dataset. Plots in the first row ((a.1) and (a.2)) use the RNN method with input of radiation and weather data. Plots in the second row ((b.1) and (b.2)) use the RNN method with input of radiation data. Plots in the third row ((c.1) and (c.2)) use the moving average method. In each plot, the top subplot illustrates the true value and the predicted value of background radiation, and the bottom subplot illustrates the absolute prediction error.

the background radiation at the beginning of the precipitation and over estimate the background radiation in the end of the precipitation. The longer the time window is, the more severe under/over estimation will be. It is difficult for the moving average method to set the time win-

dow length to make a trade off between Poisson errors and the under/over estimation errors. In contrast, the RNNs performed equally well for time windows longer than 10min. It is because RNN models are able to learn the nonlinear behavior of background radiation fluctua-

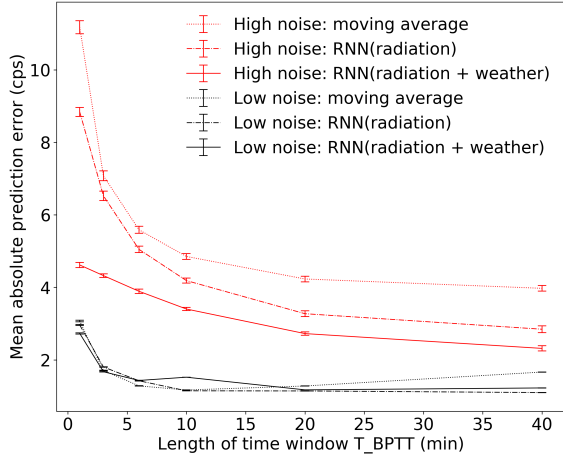


Figure 5: Mean absolute prediction error of RNNs and the moving average method under different experiment configurations. Red lines indicate models trained and tested on the high noise dataset, while black lines indicate models trained and tested on the low noise dataset. For the high noise dataset, the RNNs with radiation and weather data performed the best at all time windows. For the low noise dataset, these three models performed equally well in terms of the mean absolute prediction error.

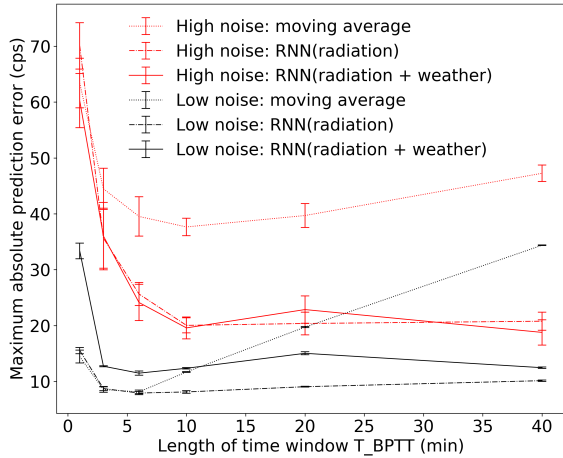


Figure 6: Maximum absolute prediction error of RNNs and the moving average method under different experiment configurations. Red lines indicate models trained and tested on the high noise dataset, while black lines indicate models trained and tested on the low noise dataset. As time window increased, the maximum prediction errors from RNN models decreased and converged to a low level, but maximum prediction errors from the moving average method firstly decreased and then increased again.

tion during precipitations, and the under/over estimation doesn't occur in RNN models.

5. Conclusions

This paper studied the problem of background radiation prediction with RNNs. A measurement platform containing a weather station and a radiation detector was set up. RNNs were trained to predict mean radiation values using past background radiation and weather measurements. With the high noise dataset, the RNN method with radiation data performed better than the moving average method in the radiation prediction task, and weather data further improved the prediction accuracy of RNN models at all time windows. With the low noise dataset, the RNN method with radiation data performed as good as the moving average method at their optimized time window. Adding weather data into the RNN models caused them to overfit to the training data. In the future, more radiation and weather data will be acquired to correct the overfitting issue. Additionally, for both high noise dataset and low noise dataset, the RNN methods showed better and more stable performance when the window size increased, which had the advantage in real application to facilitate the choice of window size parameter.

References

- [1] A. Gunatilaka, B. Ristic, R. Gailis, On localisation of a radiological point source, in: Information, Decision and Control, 2007. IDC '07, 2007, pp. 236–241. doi:[10.1109/IDC.2007.374556](https://doi.org/10.1109/IDC.2007.374556).
- [2] M. Chandy, C. Pilotto, R. McLean, Networked sensing systems for detecting people carrying radioactive material, in: Networked Sensing Systems, 2008. INSS 2008. 5th International Conference on, 2008, pp. 148–155. doi:[10.1109/INSS.2008.4610916](https://doi.org/10.1109/INSS.2008.4610916).
- [3] B. Deb, Iterative estimation of location and trajectory of radioactive sources with a networked system of detectors, IEEE Transactions on Nuclear Science 60 (2) (2013) 1315–1326. doi:[10.1109/TNS.2013.2247060](https://doi.org/10.1109/TNS.2013.2247060).
- [4] E. w. Bai, A. Heifetz, P. Raptis, S. Dasgupta, R. Mudumbai, Maximum likelihood localization of radioactive sources against a highly fluctuating background, IEEE Transactions on Nuclear Science 62 (6) (2015) 3274–3282. doi:[10.1109/TNS.2015.2497327](https://doi.org/10.1109/TNS.2015.2497327).
- [5] M. Morelande, B. Ristic, A. Gunatilaka, Detection and parameter estimation of multiple radioactive sources, in: Information Fusion, 2007 10th International Conference on, IEEE, 2007, pp. 1–7.
- [6] M. R. Morelande, B. Ristic, Radiological source detection and localisation using bayesian techniques, IEEE Transactions on Signal Processing 57 (11) (2009) 4220–4231.
- [7] J.-F. Mercier, B. Tracy, R. d'Amours, F. Chagnon, I. Hoffman, E. Korpach, S. Johnson, R. Ungar, Increased environmental gamma-ray dose rate during precipitation: a strong correlation

- with contributing air mass, *Journal of Environmental Radioactivity* 100 (7) (2009) 527–533.
- [8] R. Livesay, C. S. Blessinger, T. Guzzardo, P. Hausladen, Rain-induced increase in background radiation detected by Radiation Portal Monitors, *Journal of Environmental Radioactivity* 137 (2014) 137–141.
 - [9] N. Fujinami, Observational study of the scavenging of radon daughters by precipitation from the atmosphere, *Environment International* 22 (1996) 181–185.
 - [10] P. E. Fehlau, An applications guide to pedestrian SNM monitors, Los Alamos National Laboratory, 1986.
 - [11] R. J. Williams, J. Peng, An efficient gradient-based algorithm for on-line training of recurrent network trajectories, *Neural Computation* 2 (4) (1990) 490–501.
 - [12] Y. Bengio, P. Simard, P. Frasconi, Learning long-term dependencies with gradient descent is difficult, *IEEE Transactions on Neural Networks* 5 (2) (1994) 157–166.
 - [13] S. Hochreiter, J. Schmidhuber, Long short-term memory, *Neural Computation* 9 (8) (1997) 1735–1780.
 - [14] F. A. Gers, J. Schmidhuber, F. Cummins, Learning to forget: Continual prediction with LSTM.
 - [15] A. Graves, Generating sequences with recurrent neural networks, arXiv preprint arXiv:1308.0850.
 - [16] Y. Gal, Z. Ghahramani, A theoretically grounded application of dropout in recurrent neural networks, in: *Advances in Neural Information Processing Systems*, 2016, pp. 1019–1027.
 - [17] J. Bergstra, Y. Bengio, Random search for hyper-parameter optimization, *Journal of Machine Learning Research* 13 (Feb) (2012) 281–305.
 - [18] D. Kingma, J. Ba, Adam: A method for stochastic optimization, arXiv preprint arXiv:1412.6980.
 - [19] M. Abadi, A. Agarwal, P. Barham, E. Brevdo, Z. Chen, C. Citro, G. S. Corrado, A. Davis, J. Dean, M. Devin, S. Ghemawat, I. Goodfellow, A. Harp, G. Irving, M. Isard, Y. Jia, R. Jozefowicz, L. Kaiser, M. Kudlur, J. Levenberg, D. Mané, R. Monga, S. Moore, D. Murray, C. Olah, M. Schuster, J. Shlens, B. Steiner, I. Sutskever, K. Talwar, P. Tucker, V. Vanhoucke, V. Vasudevan, F. Viégas, O. Vinyals, P. Warden, M. Wattenberg, M. Wicke, Y. Yu, X. Zheng, TensorFlow: Large-scale machine learning on heterogeneous systems, software available from tensorflow.org (2015).
URL <http://tensorflow.org/>
 - [20] F. Chollet, et al., Keras, <https://github.com/fchollet/keras> (2015).

Appendix A. RNN structures selected by the random search algorithm.

The L1 (or L2) column denotes the output dimensions in the first (or second) LSTM layer. The Dp1 (or Dp2) column denotes the dropout rate for the first (or second) LSTM layer.

Table A.1: RNNs with radiation and weather data as input

Dataset	T_{BPTT}	L1	Dp1	L2	Dp2
Dataset A	1	1024	0	64	0
	3	256	0	16	0.5
	6	256	0	256	0.5
	10	256	0	256	0.5
	20	1024	0	16	0
	40	256	0	256	0.5
(high noise)	1	256	0	1024	0
	3	256	0	256	0.5
	6	64	0	16	0
	10	1024	0	256	0
	20	256	0	256	0.5
	40	1024	0	64	0.5
Dataset B	1	256	0	1024	0
	3	256	0	256	0.5
	6	64	0	16	0
	10	1024	0	256	0
	20	256	0	256	0.5
	40	1024	0	64	0.5
(low noise)	1	256	0	1024	0
	3	256	0	256	0.5
	6	64	0	16	0
	10	1024	0	256	0
	20	256	0	256	0.5
	40	1024	0	64	0.5

Table A.2: RNNs with radiation data as input

Dataset	T_{BPTT}	L1	Dp1	L2	Dp2
Dataset A	1	64	0	256	0
	3	1024	0	16	0
	6	1024	0	256	0.5
	10	64	0	1024	0.5
	20	1024	0	64	0
	40	256	0	64	0
(high noise)	1	256	0	256	0
	3	256	0	1024	0
	6	1024	0	64	0
	10	1024	0	256	0.5
	20	1024	0	64	0
	40	256	0	1024	0.5
Dataset B	1	256	0	256	0
	3	256	0	1024	0
	6	1024	0	64	0
	10	1024	0	256	0.5
	20	1024	0	64	0
	40	256	0	1024	0.5
(low noise)	1	256	0	256	0
	3	256	0	1024	0
	6	1024	0	64	0
	10	1024	0	256	0.5
	20	1024	0	64	0
	40	256	0	1024	0.5